shifts are converted into a contrast in energy by using a long wavelength pass filter followed by a conventional photodetector operating at speeds comparable to the repetition rate of the system. By optimally choosing the average power and the filter cutoff wavelength, a high contrast ratio is obtained. The contrast ratio is defined as the ratio of the energy of the uncoded pulses to that of the coded pulses at the output of the thresholder. As seen in Fig. 3, a contrast ratio of nearly 1000 is achieved for a 1569nm cutoff wavelength, a 0.44mW average power for a fixed M-sequence code. It should be noted that the higher contrast ratio at longer cutoff wavelengths comes at the expense of lower energy at the output of the thresholder. Fig. 4 shows the conversion efficiency of the nonlinear thresholder defined as the ratio of the energy at the output of the thresholder to the energy at the input of the thresholder. As shown in the Figure, for 0.44mW average power at the thresholder input, we get almost 50% conversion efficiency for lower cutoff wavelengths, but the efficiency drops down to ~10% when the cutoff wavelength is ~1569nm.

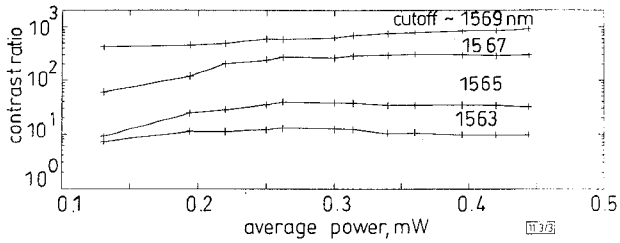

Fig. 3 *Contrast ratio of nonlinear receiver for different cutoff wavelengths of long wavelength pass filter against average signal power at input of nonlinear thresholder fibre*

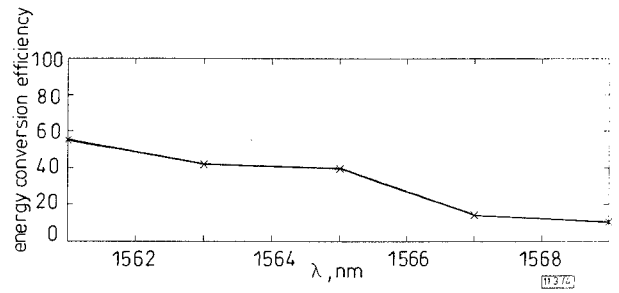

Fig. 4 *Energy conversion efficiency of nonlinear thresholder for different cutoff wavelengths of long wavelength pass filter*

Average signal power at input of thresholder fibre is 0.44mW

In conclusion we have demonstrated a nonlinear fibre optic receiver for ultrashort pulse CDMA systems which can operate at received pulse energies as low as ~1pJ. The receiver has an internal erbium fibre preamplifier, a fibre pigtailed pulse shaper decoder, a passive fibre where nonlinear frequency shifts occur and a long wavelength pass filter. The receiver has a contrast ratio of nearly 1000 and a conversion efficiency of nearly 10%. In the future it should be possible to obtain even higher contrast ratios by including hard spectral apertures within the pulse shaper/decoder and to demonstrate similar thresholder concepts based on soliton self-frequency shifts in fibres with λ_0 at shorter wavelengths. We also intend to use these thresholders in system experiments testing ultrashort pulse CDMA systems over distances suitable for local area networks.

Acknowledgments: The authors gratefully acknowledge C.C. Chang for building the fibre ring laser, M. Newhouse and V. Da Silva of Corning Inc. for supplying erbium doped and dispersion shifted fibres, A. Vengsarkar and D. Peckham of Bell Labs. for supplying the dispersion compensating fibre and I. Duling of Naval Research Labs. for helpful discussions related to erbium amplifiers. This work was supported by the National Science Foundation under grants ECS-9626967 and ECS-9312256.

30 January 1997
Electronics Letters Online No: 19970416

H.P. Sardesai and A.M. Weiner (*School of Electrical and Computer Engineering, Purdue University, 1285 Electrical Engineering Building, West Lafayette, Indiana 47907-1285, USA*)

References

1 SALEHI, J.A., WEINER, A.M., and HERITAGE, J.P.: 'Coherent ultrashort light pulse code-division multiple access communication systems', *J. Lightwave Technol.*, 1990, **8**, (3), pp. 478–491
2 WEINER, A.M.: 'Femtosecond optical pulse shaping and processing', *Progress in Quantum Elect.*, 1995, **19**, (3), pp. 161–237
3 TAMURA, K., IPPEN, E.P., HAUS, H.A., and NELSON, L.E.: '77-fs pulse generation from a stretched-pulse modelocked all-fibre ring laser', *Opt. Lett.*, 1993, **18**, (13), pp. 1080–1082
4 WEINER, A.M., LEAIRD, D.S., PATEL, J.S., and WULLERT, J.R.: 'Programmable shaping of femtosecond optical pulses by use of a 128-element liquid crytstal phase modulator', *IEEE J. Quantum Electron.*, 1992, **28**, (4), pp. 908–920
5 AGRAWAL, G.P., and POTASEK, M.J.: 'Nonlinear pulse distortion in single-mode optical fibres at zero-dispersion wavelength', *Phys. Rev. A.*, 1986, **33**, (3), pp. 1765–1776
6 STERN, M., HERITAGE, J.P., ANDERSON, W.T., and KILMER, J.: 'Soliton technique to characterize single-mode fibre dispersion', *J. Lightwave Technol.*, 1992, **10**, (12), pp. 1777–1779

Reflection-type normally-on two-wavelength modulator

Chia-Ming Tsai and Chien-Ping Lee

Indexing terms: Semiconductor quantum wells, Optical modulation

The authors demonstrate a novel reflection-type normally-on two-wavelength modulator by combining two quantum-well structures with different operating wavelengths in a coupled cavity structure. Reflection spectra show simultaneous modulations at wavelengths of 856 and 886 nm in the device consisting of GaAs/AlGaAs and InGaAs/AlGaAs quantum wells for each wavelength. Under separate applied voltages, maximum reflectivity changes of 70 and 54% were obtained for the two wavelengths. To the best of the authors' knowledge, this is the first two-wavelength reflection modulator ever reported.

Surface-normal quantum well modulators based on quantum confined Stark effect (QCSE) have become one of the key devices in many applications, such as optical communications [1] and interconnections [2], optical switching networks [3], and optical data processing applications using e.g. smart pixels [4], because of their excellent performance and compatibility with other semiconductor optoelectronic devices. All the modulators developed so far are for single-wavelength operation. However, in future WDM or multichannel systems, transmission of multiple wavelengths is needed. Although multichannel laser diodes have been developed [5 – 9], modulators which are capable of handling two wavelengths or more have not been reported. In this Letter, we report for the first time a two-wavelength reflection-type quantum well modulator. We believe that this new device will provide much more flexibility for future system applications.

To achieve a two-wavelength modulator, two types of quantum wells with different operating wavelengths must be used simultaneously in one structure. But if these two modulators are put inside one simple conventional cavity, the quantum wells designed for long wavelength will absorb the short-wavelength photons, and the resonant condition cannot be tailored for both wavelengths. So, it is almost impossible to achieve a reasonable modulation performance. In our devices, a coupled-cavity design is used. The quantum wells for the short wavelength operation are placed in front of the quantum wells designed for the long wavelength and an additional reflector is placed in between to prevent short wavelength light penetrating into the lower quantum wells. For long-wavelength operation, another high-reflection mirror is added behind the long-wavelength quantum-well region to achieve a complete AFP cavity structure.

The two-wavelength modulator is shown as a schematic diagram in Fig. 1. It is similar to that of a coupled cavity modulator [10, 11]. But in our structure, we place the short-wavelength quantum-well absorbing layer in the front cavity. Because of the middle reflector and the large absorption coefficient of the quantum wells

in the rear cavity, the modulation characteristics for the short wavelength are determined mostly by the front cavity and the rear cavity does not play any important role. For long wavelength operation, however, the whole device structure acts like a coupled cavity because the front quantum wells are transparent at this wavelength. From the explanation given above, it can be see that the whole structure needs to be designed in such a way so that the front cavity satisfies the resonant condition for the short wavelength light and both the front cavity and the rear cavity satisfy the resonant condition for long wavelength light.

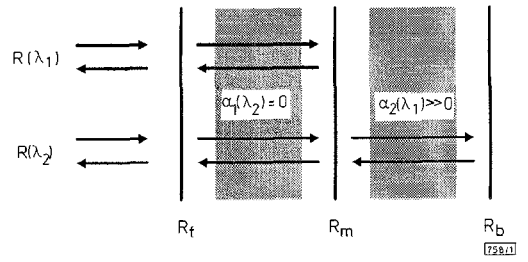

Fig. 1 *Mechanism of two-wavelength operation*

After understanding the basics of achieving two-wavelength operation, we designed and fabricated a two-wavelength modulator. The short wavelength quantum wells were built with GaAs/AlGaAs. For long wavelength operation, we chose InGaAs/AlGaAs quantum wells. The complete layer structure of a fabricated device is shown in Fig. 2. The middle reflector consists of a 10 pair DBR stack. This reflector design results in a high-reflection band with reflectivity over 80% covering a range from 850 to 930nm. After considering the coupling effect, an effective reflectivity of ~60% is derived from our calculation for long-wavelength operation. The whole structure was grown by an MBE system.

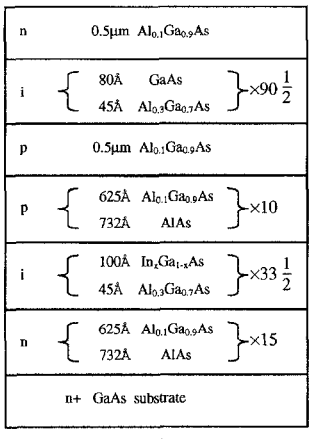

Fig. 2 *Complete layer structure of two-wavelength modulator*

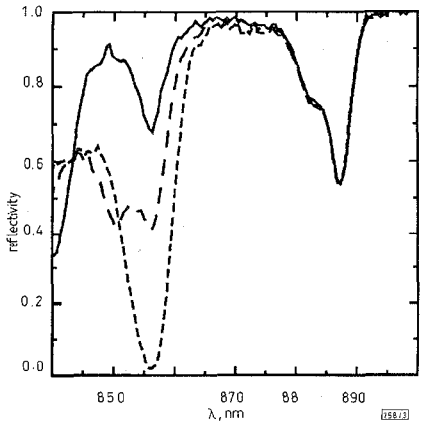

Fig. 3 *Reflection spectra of two-wavelength modulator under various biasing voltages on upper short-wavelength QWs*

——— 0V, — — 15V, – – – – 19V

The growth started with 15 periods of $Al_{0.1}Ga_{0.9}As$ (625Å)/AlAs (732Å) DBR mirror which was followed by 33 periods of $In_xGa_{1-x}As$ (100Å)/$Al_{0.3}Ga_{0.7}As$ (45Å) quantum wells designed for long-wavelength operation. The growth procedure was then interrupted and an *in-situ* reflection spectrum was measured. The measured excitonic wavelength was near 870nm, which was somewhat shorter than what we expected in advance. An important matching procedure in layer thickness then followed, to reach resonance at the desired operating wavelength. Here, a wavelength of 885nm was chosen. At the middle reflector and then the short-wavelength quantum-well region, 90 periods of GaAs (80Å)/$Al_{0.3}Ga_{0.7}As$ (45Å), were sequentially grown on the matched cavity structure. The non-biased excitonic wavelength was 840nm. The second operating wavelength we chose here was 855nm. By adjusting the layer thickness for simultaneous operations at 885 and 855nm, the total thickness was ~6μm.

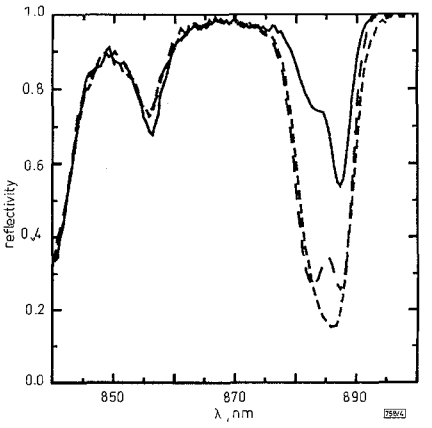

Fig. 4 *Reflection spectra of two-wavelength modulator under various biasing voltages on lower long-wavelength QWs*

——— 0V, — — 4V, – – – – 5V

After layer growth, the device was fabricated by two mesa-etching steps to separately define the ohmic contact for each modulator. Figs. 3 and 4 show the modulated reflection spectra with each modulator biased separately. As clearly shown in the Figures, the two-wavelength operation at wavelengths of 856 and 886nm was achieved. Each modulator operated almost independently without any significant crosstalk. For operation at 856nm, an excellent reflectivity change of 70% was obtained for a bias voltage of 19V. The high voltage needed was due to the relatively thicker GaAs/$Al_{0.3}Ga_{0.7}As$ quantum-well region and the narrow well design. For the 886nm operation, however, only 5V was needed to cause a 54% change in reflectivity. This is because a thinner $In_xGa_{1-x}As$/$Al_{0.3}Ga_{0.7}As$ quantum-well region was used. We noticed a small reflectivity change at a short operating wavelength of 856nm during long wavelength operation. This is caused by the modulation of absorption intensity in the bottom quantum-well region owing to the residual coupling effect resulted from reflection of the bottom cavity. This can be totally eliminated by introducing an intermediate blocking layer, which is transparent at 886nm but strongly absorptive at 856nm, between the middle reflector and the bottom quantum-well region. The relatively large off-state reflectivity of 15% at 886nm is due to insufficient thickness of the quantum-well absorbing layer. As we can see, the operating voltages at the two wavelengths were very different from each other. This mainly arises from the unbalanced cavity confinement scheme used here and can be solved using a modified middle reflector design.

In conclusion, we have successfully fabricated a new reflection-type normally-on two-wavelength modulator. A special coupled cavity design and two different quantum well absorption regions have resulted in two-wavelength operation at 856 and 886nm. The maximum reflectivity changes obtained were 70 and 54% for the two wavelengths, respectively.

Acknowledgment: This work was supported by the National Science Council of the Republic of China under contract NSC86-2215-E009-010.

19 December 1996
Electronics Letters Online No: 19970405

Chia-Ming Tsai and Chien-Ping Lee (*Department of Electronics Engineering and Institute of Electronics, National Chiao Tung University, Hsin-Chu 300, Taiwan, Republic of China*)

References

1 BARRON, C.C., MAHON, C.J., THIBEAULT, B.J., WANG, G., JIANG, W., COLDREN, L.A., and BOWERS, J.E.: 'Millimeter-wave asymmetric Fabry-Perot modulators', *IEEE J. Quantum Electron.*, 1995, **31**, (8), pp. 1484–1493

2 MOSELEY, A.J., KEARLEY, M.Q., MORRIS, R.C., ROBBINS, D.J., THOMPSON, J., and GOODWIN, M.J.: 'Uniform 8×8 aray InGaAs/Inp multiquantum well asymmetric Fabry-Perot modulators for flipchip solder bond hybrid optical interconnect', *Electron. Lett.*, 1992, **28**, (1), pp. 12–14

3 MIDWINTER, J.E.: 'Novel approach to the design of optically activated wideband switching matrices', *IEE Proc.*, 1987, **134**, pp. 261–268

4 LENTINE, A.C., and MILLER, D.A.B.: 'Evolution of the SEED technology: bistable logic gates to optoelectronic smart pixels', *IEEE J. Quantum Electron.*, 1993, **29**, (2), pp. 655–669

5 : 'Special issue on All-Optical Networks', *J. Lightwave Technol.*, July 1993, **LT**,

6 TSANG, W.T., KAPRE, R.M., LOGAN, R.A., and TANBUN-EK, T.: 'Control of lasing wavelength in distributed feedback lasers by angling the active stripe with respect to the grating', *IEEE Photonics Technol. Lett.*, 1993, **5**, (9), pp. 978–980

7 KUZNETSOV, M., VERLANGGIERI, P., and DENTAI, A.G.: 'Frequency tuning characteristics and WDM channel access of the semiconductor three-branch Y3-lasers', *IEEE Photonics Technol. Lett.*, 1994, **6**, (2), pp. 157–160

8 KOYAMA, F., MUKAIHARA, T., HAYASHI, Y., OHNOKI, N., HATORI, N., and IGA, K.: 'Wavelength control of vertical cavity surface-emitting lasers by using nonplanar MOCVD', *IEEE Photonics Technol. Lett.*, 1995, **7**, (1), pp. 10–12

9 LI, G.P., MAKINO, T., and WU, C.M.: 'Multi-λ ridge waveguide gain-coupled DFB laser array,', *J. Lightwave Technol.*, 1995, **13**, (2), pp. 196–199

10 FRITZ, I.J., KLEM, J.F., and WENDT, J.R.: 'Reflectance modulator based on tandem Fabry-Perot resonators', *Appl. Phys. Lett.*, 1991, **59**, (7), pp. 753–755

11 LAW, K.K.: 'Characteristics of absorption Fabry-Perot modulators due to the influence of coupled cavities', *J. Appl. Phys.*, 1995, **77**, (5), pp. 1864–1867

System design and performance of reconfigurable and simultaneous 2D multiple-plane WDM optical interconnects

J.E. Leight, J. Yoo and A.E. Willner

Indexing terms: Wavelength division multiplexing, Optical interconnections

A system design for reconfigurable and simultaneous 2D multiple-plane WDM optical interconnects has been investigated. Device characteristics such as detector responsivity shape, efficiency, and complexity affect the design requirements for wavelength separation and channel power. With decreasing wavelength separation, increased optical crosstalk and signal power loss result in performance penalties most notably for the middle wavelength channels. When signal power loss and optical crosstalk from the detection of undesired channels are evaluated, it is found that wavelength channel spacing down to 10nm can be tolerated for the specific detector responsivity shape and efficiency attainable from currently available devices.

We have previously proposed and experimentally demonstrated WDM multiple-plane optical interconnects [1, 2] as one possible method of establishing reconfigurable or simultaneous switching for ultra-high throughput systems such as supercomputing or large-scale signal processing applications. The conceptual WDM interconnect, shown in Fig. 1*a*, utilises a 2D *N*×*N* pixel array of identical multiple-wavelength VCSEL arrays for the transmitting plane and incorporates wavelength-selectivity into a 2D *N*×*N* pixel array of photodetectors for each subsequent receiving plane. At each wavelength-selective receiving plane, the intended signal is detected and signals at longer wavelengths pass through to be detected at the following planes. When only a single wavelength of the transmitting pixel is operated, the interconnect is reconfigurable as the wavelength of the signal determines which of the detecting planes receive data. When multiple-wavelength outputs of a transmitting pixel are all 'ON', simultaneous communication to many planes is possible. System penalties are the result of power loss from unintended signal detection at previous planes and optical crosstalk from the detection of undesired channels.

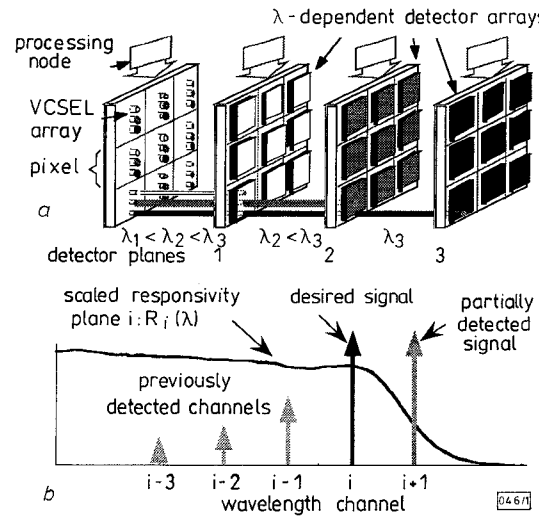

Fig. 1 *WDM multiple-plane optical interconnect and representative signal powers and measured detector spectra illustrating detection at one plane*

a WDM multipleplane optical interconnect
b Representative signal powers and measured detector spectra

Understanding the source and characteristics of system penalties in WDM optical interconnects is important in establishing designs to optimise system performance and functionality. We have determined the dependence of optical crosstalk and signal power penalties on wavelength channel separation and channel power for various five-wavelength WDM multiple-plane optical interconnects. Five wavelengths are adequate to illustrate how device characteristics such as detector responsivity shape, efficiency, and complexity impact system performance and the choice of design parameters. With decreasing wavelength separation, increased optical crosstalk and signal power loss result in performance penalties most notably for the middle wavelength channels. When signal power loss and optical crosstalk from the detection of undesired channels are evaluated, it is found that wavelength channel spacing down to 10 nm can be tolerated for the specific detector responsivity shape and efficiency attainable from currently available devices.

To determine crosstalk and signal power penalties for WDM interconnects, we find channel power and signal detection throughout the interconnect system. Our modelling is based on measured detector responsivity data and semi-empirical expressions for GaAs material parameters (α, n) that match well with published experimental data [3 – 6]. The detector planes are assumed to consist of $In_xGa_{1-x}As$ detectors with responsivity curves determined by shifting the measured responsivity data for a GaAs detector to longer wavelengths. The shape of the response rolloff, a result of detector design and material characteristics, determines the wavelength selectivity of the detector and determines the extent of power penalties and optical crosstalk. Fig. 1*b* illustrates the optical spectrum for detection of a desired signal and undesired interfering channels, using the measured responsivity data and representative signal power levels, at one plane of the interconnect. The peak responsivity is related to the detecting efficiency which would in practice be a function of detector thickness. At each plane, the power and corresponding responsivity for each wavelength signal illuminating the detector is used to calculate the signal power loss referenced to the transmitting plane and the crosstalk penalty. The crosstalk penalty is given by $I_{sig}(I_{sig} - I_{int})$